Bound States of the Cl(^2P)−HCl van der Waals Complex from Coupled ab Initio Potential Energy Surfaces

W. B. Zeimen, J. Kłos, G. C. Groenenboom, and A. van der Avoird*

Institute of Theoretical Chemistry, NSRIM, University of Nijmegen, Toernooiveld 1, 6525 ED Nijmegen, The Netherlands

Received: February 25, 2003; In Final Form: May 1, 2003

With the use of recently computed diabatic potential energy surfaces (*J. Chem. Phys.* **2001**, *115*, 3085) a full ab initio calculation was made of the bound energy levels of the Cl(^2P)−HCl van der Waals complex for total angular momentum $J = {}^1/_2, {}^3/_2, {}^5/_2$, and ${}^7/_2$. The dissociation energy D_0 of the complex was found to be 337.8 cm^{-1} for $J = {}^1/_2$ and $|\Omega| = {}^1/_2$, where Ω is the projection of $\boldsymbol{J}$ on the Cl−HCl bond axis. The complex is T-shaped in the ground state and in a series of stretch and bending excited states, with a van der Waals bond length R of ∼3.2 Å. A series of states with linear geometry were also found, however, with $|\Omega| = {}^3/_2$ and $R \approx 3.9$ Å, the lowest of which has a binding energy of 276.1 cm^{-1}. The rovibronic levels were analyzed with the help of one-dimensional calculations with R fixed at values ranging from 2.5 to 5.5 Å and the use of diabatic and adiabatic potential energy surfaces that both include the important spin−orbit coupling. The states of linear geometry are in qualitative agreement with previous work based on more approximate potential energy surfaces; the T-shaped states of considerably lower energy were not predicted earlier. Analysis of the rotational structure and parity splitting of the rovibronic levels leads to the remarkable observation that this T-shaped complex shows several features typical of a linear open-shell molecule.

Introduction

A chemical reaction that has been studied intensively over more than a decade, both by theory[1−10] and by experiment,[11−20] is the hydrogen exchange reaction between a free Cl atom in its ground ^2P state and the HCl molecule. A weakly bound Cl(^2P)−HCl van der Waals complex is present in the entrance and exit channels of this reaction, which is believed to influence the rate and outcome of the reaction.[21] Theoretical studies of the bound states of this complex were reported by Dubernet and Hutson[22] and, more recently, by Zdanska et al.[23] Dubernet and Hutson based their studies on diabatic model potentials, which they constructed by combining empirical Ar−HCl, Ar−Cl, and Ar−Ar potentials with the electrostatic interactions between the quadrupole moment of the Cl(^2P) atom and the dipole and quadrupole of HCl. Zdanska and co-workers calculated adiabatic potential energy surfaces at the multireference averaged coupled-pair functional (MRACPF) level and reported bound states calculated with and without inclusion of an angular first-derivative non-adiabatic coupling term. In their calculations they fixed the orientation of the intermolecular vector $\boldsymbol{R}$ between the Cl nucleus and the HCl center of mass, which corresponds approximately, but not exactly, to a neglect of the overall rotation of the complex.

Accurate two-dimensional (2D) adiabatic and diabatic potential energy surfaces for the Cl(^2P)−HCl system were recently reported by Kłos et al.[24] They were obtained from ab initio spin-restricted coupled cluster calculations with single, double, and noniterative triple excitations [RCCSD(T)], combined with multireference configuration interaction including single and double excitations (MRCISD) to obtain the non-adiabatic coupling coefficient. In the present work we re-expand these diabatic potentials in the form that was derived in refs 22 and 25−27 and apply them in a detailed study of the bound states of the Cl(^2P)−HCl van der Waals complex. The method for the calculation of the van der Waals levels is described under Bound State Calculations. Also, the spin−orbit interaction in the Cl(^2P) atom is included in this calculation, with the same assumption as in refs 22 and 23 that the spin−orbit coupling constant is not affected by the weak interaction with the HCl molecule. We obtain a full solution of the 2D problem with all six electronic states of Cl(^2P)−HCl that correlate asymptotically to the $^2P_{3/2}$ and $^2P_{1/2}$ spin−orbit states of the Cl atom. To understand the character of the bound states on the multiple potential surfaces, we also perform a set of rigid bender calculations with the Cl−HCl distance R frozen, to a range of values. Under Results we discuss and compare our findings with previous work. In the final section, our conclusions are summarized.

Bound State Calculations

The bound states of Cl(^2P)−HCl are most conveniently calculated in a two-angle embedded body-fixed (BF) frame with the z-axis along the vector $\boldsymbol{R}$ from the Cl atom to the HCl center of mass. This frame is related to a space-fixed (SF) frame by a rotation over the angles (β,α), which are the polar angles of $\boldsymbol{R}$ with respect to the SF frame. The Cl−H bond axis $\boldsymbol{r}$ has the polar angles (θ,ϕ) with respect to the BF frame; θ is the angle between $\boldsymbol{r}$ and $\boldsymbol{R}$, which is zero for the linear Cl−HCl geometry. Because the H−Cl vibration has a much higher frequency than the vibrations of the Cl−HCl complex, we froze the H−Cl bond length r and used the experimental value for the ground state rotational constant $b_0 = 10.44019$ cm^{-1} of HCl. The ab initio potential was calculated for the equilibrium bond length $r_e = 1.275$ Å. In this representation the Hamiltonian for the nuclear motion on the multiple diabatic potential surfaces reduces to

10.1021/jp034475z CCC: $25.00
Published on Web 06/04/2003

$$\hat{H} = \frac{-\hbar^2}{2\mu_{AB}R}\frac{\partial^2}{\partial R^2}R + \frac{(\hat{\boldsymbol{j}}_A + \hat{\boldsymbol{j}}_B)^2 - 2(\hat{\boldsymbol{j}}_A + \hat{\boldsymbol{j}}_B)\cdot\hat{\boldsymbol{J}} + \hat{J}^2}{2\mu_{AB}R^2} + b_0\hat{j}_B^{\,2} + A\hat{\boldsymbol{\lambda}}\cdot\hat{\boldsymbol{S}} + \sum_{\mu',\mu}|\lambda,\mu'\rangle\, V_{\mu',\mu}(R,\theta,\phi)\,\langle\lambda,\mu| \quad (1)$$

where $\mu_{AB} = 17.732802$ u is the reduced mass of the complex. The operators $\hat{\boldsymbol{\lambda}}$ and $\hat{\boldsymbol{S}}$ represent the orbital and spin angular momenta of the Cl atom and $\hat{\boldsymbol{j}}_A = \hat{\boldsymbol{\lambda}} + \hat{\boldsymbol{S}}$ the total atomic angular momentum. The splitting between the ground $j_A = {}^3/_2$ and excited $j_A = {}^1/_2$ spin−orbit states of Cl(^2P) is $D_{SO} = 882.4$ cm^{-1} and the atomic spin−orbit coupling constant is $A = -2D_{SO}/3 = -588.27$ cm^{-1}. The operator $\hat{\boldsymbol{j}}_B$ is the rotational angular momentum of the HCl molecule and $\hat{\boldsymbol{J}}$ the total angular momentum of the complex. The diabatic states of the Cl(^2P)−HCl complex that correlate with the corresponding states of the Cl(^2P) atom are labeled with the quantum numbers (λ,μ), where $\lambda = 1$ and $\mu = -1, 0, 1$ is the projection of $\hat{\boldsymbol{\lambda}}$ on the BF z-axis $\boldsymbol{R}$. The potentials $V_{\mu',\mu}(R,\theta,\phi)$ are the diabatic interaction potentials in a two-angle embedded BF frame as described in ref 27. The expansion of these diabatic potentials is given by the following expression:

$$V_{\mu',\mu}(R,\theta,\phi) = \langle\lambda,\mu'|\hat{V}|\lambda,\mu\rangle = \sum_{l_B} C_{l_B,\mu-\mu'}(\theta,\phi)\, v_{l_B}^{\mu',\mu}(R) \quad (2)$$

The functions $C_{l,m}(\theta,\phi)$ are Racah normalized spherical harmonics. Note that only functions with $m = \mu - \mu'$ occur in the expansion. The same formula (eq 2) with identical expansion coefficients holds in a three-angle embedded BF frame with $\phi = 0$[27] and the potentials $V_{\mu',\mu}(R,\theta) \equiv V_{\mu',\mu}(R,\theta,0)$ do not depend on the angle ϕ in this frame.

Accurate ab initio results for the diabatic potential surfaces $V_{\mu',\mu}(R,\theta)$ are given in ref 24. To express their anisotropy in the form of eq 2, we made new fits of the original ab initio data. For the diabatic potential surfaces $V_{0,0}$ and $V_{1,1} = V_{-1,-1}$ we fitted the R dependence to an Esposti−Werner[28] function for each value of θ on the grid of 13 angles used in the ab initio calculations. Subsequently, we obtained the anisotropic expansion coefficients $v_{l_B}^{\mu',\mu}(R)$ in eq 2 for a given R from a least-squares fit of the values for the 13 angles to a set of spherical harmonics $C_{l_B,m}(\theta,0)$ with $m = \mu - \mu' = 0$ and $l_B = 0, 1, ..., 8$. For the diabatic potential $V_{-1,1}$ we made a new global fit of the ab initio data similar to the fit made in ref 24, but with the anisotropy expanded in spherical harmonics $C_{l,m}(\theta,0)$ with $m = 2$ instead of Legendre polynomials $P_l^0(\cos\theta)$. The latter are, of course, equal to $C_{l,m}(\theta,0)$ with $m = 0$, so this seems only a subtle difference, but a correct description of the anisotropy[27] according to eq 2 requires that m is fixed at $\mu - \mu' = 2$. The short-range contribution to $V_{-1,1}$ was written as

$$V_{sr}(R,\theta) = G(R,\theta)\exp[d(\theta) - b(\theta)R] \quad (3)$$

where

$$G(R,\theta) = \sum_{l=|m|}^{l_{max}}\sum_{i=0}^{3} g_{il}R^i C_{l,m}(\theta,0) \quad (4)$$

with $m = 2$ and $l = l_B$ ranging from 2 to 9. The exponents $d(\theta)$ and $b(\theta)$ were expanded in Legendre polynomials $P_l^0(\cos\theta)$ with $l = 0, 1, 2$, just as in ref 24. The long-range contribution was represented as a damped expansion in powers of R^{-1}

$$V_{lr}(R,\theta) = \sum_{n=4}^{10}\sum_{l=|m|}^{n-4} f_n(b(\theta)R)C_{nl}R^{-n}C_{l,m}(\theta,0) \quad (5)$$

The electrostatic multipole−multipole contributions start at $n = 4$, the induction and dispersion contributions start at $n = 6$, and $f_n(bR)$ is a Tang−Toennies damping function.[29] The coefficients C_{nl} with $n = 4$ and $n = 5$ were not varied in the fit. They were determined from the quadrupole moment of Cl(^2P) and the dipole and quadrupole of HCl according to the long-range formulas in ref 27. Also for the diabatic coupling potential $V_{0,1}$ we made a new global fit, with the same procedure as applied in the fit of $V_{-1,1}$. In this case, the exponents $d(\theta)$ and $b(\theta)$ in eq 3 were chosen to be independent of θ, and we used spherical harmonics $C_{l,m}(\theta,0)$ with $m = \mu - \mu' = 1$ in the fits of eqs 4 and 5, with $l = l_B$ ranging from 1 to 6. Finally, we computed the expansion coefficients $v_{l_B}^{-1,1}(R)$ and $v_{l_B}^{0,1}(R)$ for l_B values up to 12 according to eq 2 by Gauss−Legendre numerical integration over the fitted potentials $V_{-1,1}$ and $V_{0,1}$. These coefficients obey the relations $v_{l_B}^{-1,1}(R) = v_{l_B}^{1,-1}(R)$ and $v_{l_B}^{0,1}(R) = v_{l_B}^{0,-1}(R) = -v_{l_B}^{1,0}(R) = -v_{l_B}^{-1,0}(R)$ (see ref 27), so that all diabatic potentials $V_{\mu',\mu}(R,\theta,0)$ with $\mu',\mu = -1, 0, 1$ are known.

Because of the large spin−orbit coupling in the Cl(^2P) atom it is most convenient for the interpretation of the results to use a coupled atomic basis set

$$|j_A\omega_A\rangle \equiv |(\lambda S)j_A\omega_A\rangle = \sum_{\mu,\sigma}|\lambda,\mu\rangle|S,\sigma\rangle\langle\lambda,\mu;S,\sigma|\, j_A,\omega_A\rangle \quad (6)$$

for which the spin−orbit term in the Hamiltonian $\hat{\boldsymbol{\lambda}}\cdot\hat{\boldsymbol{S}} = (\hat{j}_A^2 - \hat{\lambda}^2 - \hat{S}^2)/2$ is diagonal. The expression $\langle\lambda,\mu;S,\sigma|j_A,\omega_A\rangle$ is a Clebsch−Gordan coefficient. Because $\lambda = 1$ and $S = {}^1/_2$, one finds that $j_A = {}^1/_2$ and ${}^3/_2$. The two-angle embedded BF basis for the complex reads

$$|n,j_A,\omega_A,j_B,\omega_B,\Omega\rangle = |n\rangle\left[\frac{2J+1}{4\pi}\right]^{1/2} |\, j_A\omega_A\rangle Y_{j_B,\omega_B}(\theta,\phi)\, D^{(J)}_{M,\Omega}(\alpha,\beta,0)^* \quad (7)$$

The spherical harmonics $Y_{j_B,\omega_B}(\theta,\phi)$ describe the rotation of the HCl monomer with respect to the dimer BF frame and the symmetric rotor functions $D^{(J)}_{M,\Omega}(\alpha,\beta,0)^*$ the overall rotation of the complex. The exact quantum numbers J, M, λ, and S are omitted from the short notation on the left-hand side. The angular momentum components on the BF z-axis obey the relation $\Omega = \omega_A + \omega_B$. The radial basis functions $|n\rangle = \chi_n(R)$ are Morse oscillator type functions defined in ref 30. Formulas for the matrix elements of the Hamiltonian over this basis are given in ref 27.

In addition to J and M, the parity of the states of the complex under inversion $\hat{\imath}$ is a good quantum number. The effect of inversion on the basis is

$$\hat{\imath}|n, j_A,\omega_A, j_B,\omega_B,\Omega\rangle = (-1)^{\lambda-j_A+J}|n,j_A,-\omega_A,j_B,-\omega_B,-\Omega\rangle \quad (8)$$

This property is used to construct a parity-adapted basis

$$|n,j_A,\omega_A,j_B,\omega_B,|\Omega|,\, p\rangle = 2^{-1/2}\,[|n,j_A,\omega_A,j_B,\omega_B,\Omega\rangle + p(-1)^{\lambda-j_A+J}|n,j_A,-\omega_A,j_B,-\omega_B,-\Omega\rangle] \quad (9)$$

with parity p. It is customary to define the spectroscopic parity ϵ, which is related to the total parity by $\epsilon = p(-1)^{J-S}$. Functions

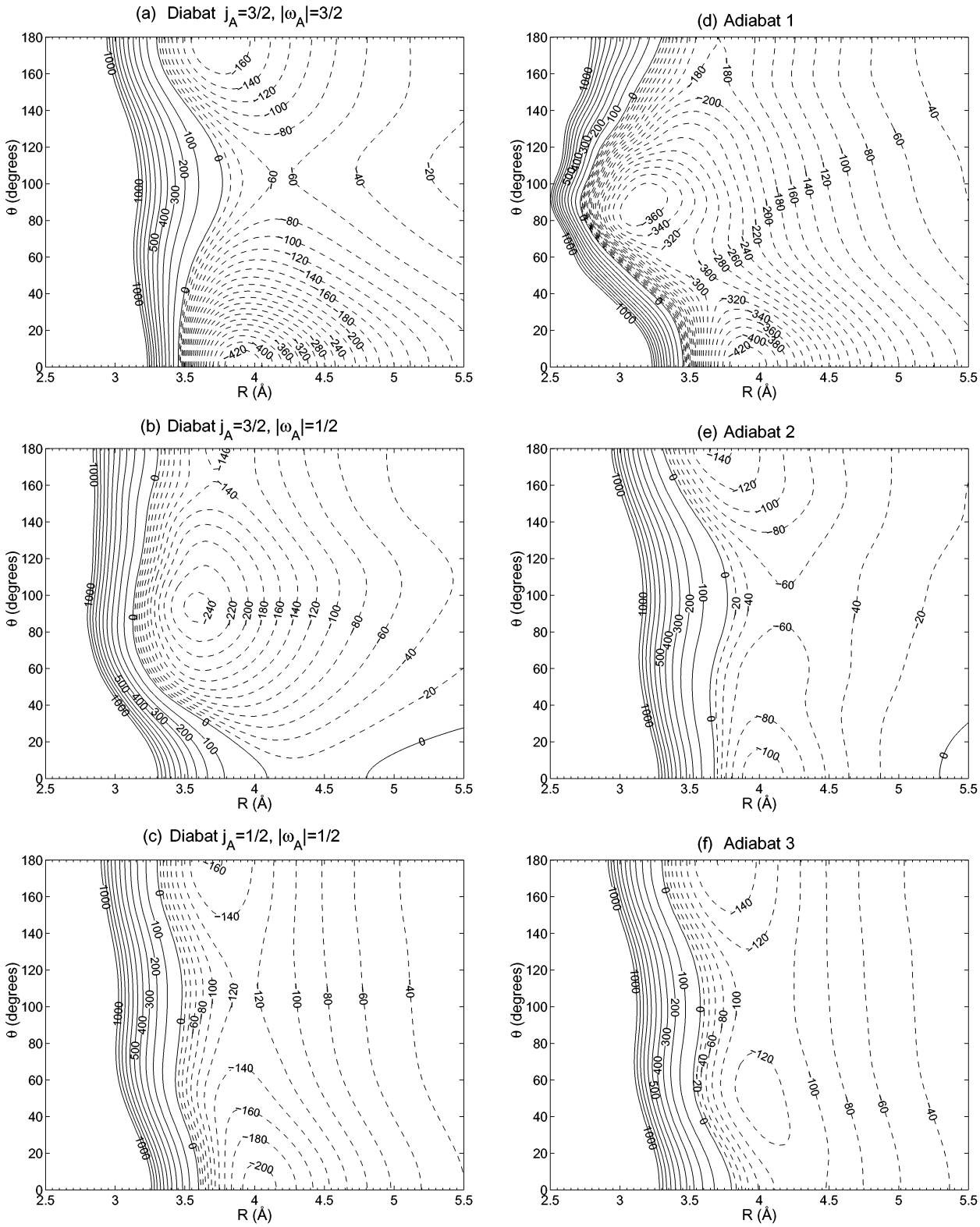

Figure 1. Diabatic $j_A = {}^3/_2$, $|\omega_A| = {}^3/_2$ (a), $j_A = {}^3/_2$, $|\omega_A| = {}^1/_2$ (b), and $j_A = {}^1/_2$, $|\omega_A| = {}^1/_2$ (c) and adiabatic (d−f) potential energy surfaces including spin−orbit coupling for the Cl(^2P)−HCl complex. Surfaces a, d, b, and e are given relative to the energy of the $^2P_{3/2}$ state of the Cl atom and surfaces c and f relative to the energy of the $^2P_{1/2}$ state.

with parities $\epsilon = 1$ and $\epsilon = -1$ are denoted with *e* and *f*, respectively.

Results

The bound states of the complex were obtained from a full diagonalization of the Hamiltonian matrix. Calculations were performed for J up to $^7/_2$ inclusive. This does not provide all of the bound states. A simple extrapolation of the lowest energy level for each J with a second-order polynomial shows that there might still be bound states for $J = {}^{123}/_2$. The levels were converged to within 10^{-4} cm^{-1} with an angular basis truncated at $j_{B_{max}} = 15$ and a radial basis with $n_{max} = 14$. Test calculations with $j_{B_{max}} = 20$ gave levels that did not deviate by $>10^{-6}$ cm^{-1} from the $j_{B_{max}} = 15$ results.

It is important for understanding the bound levels of Cl(^2P)−

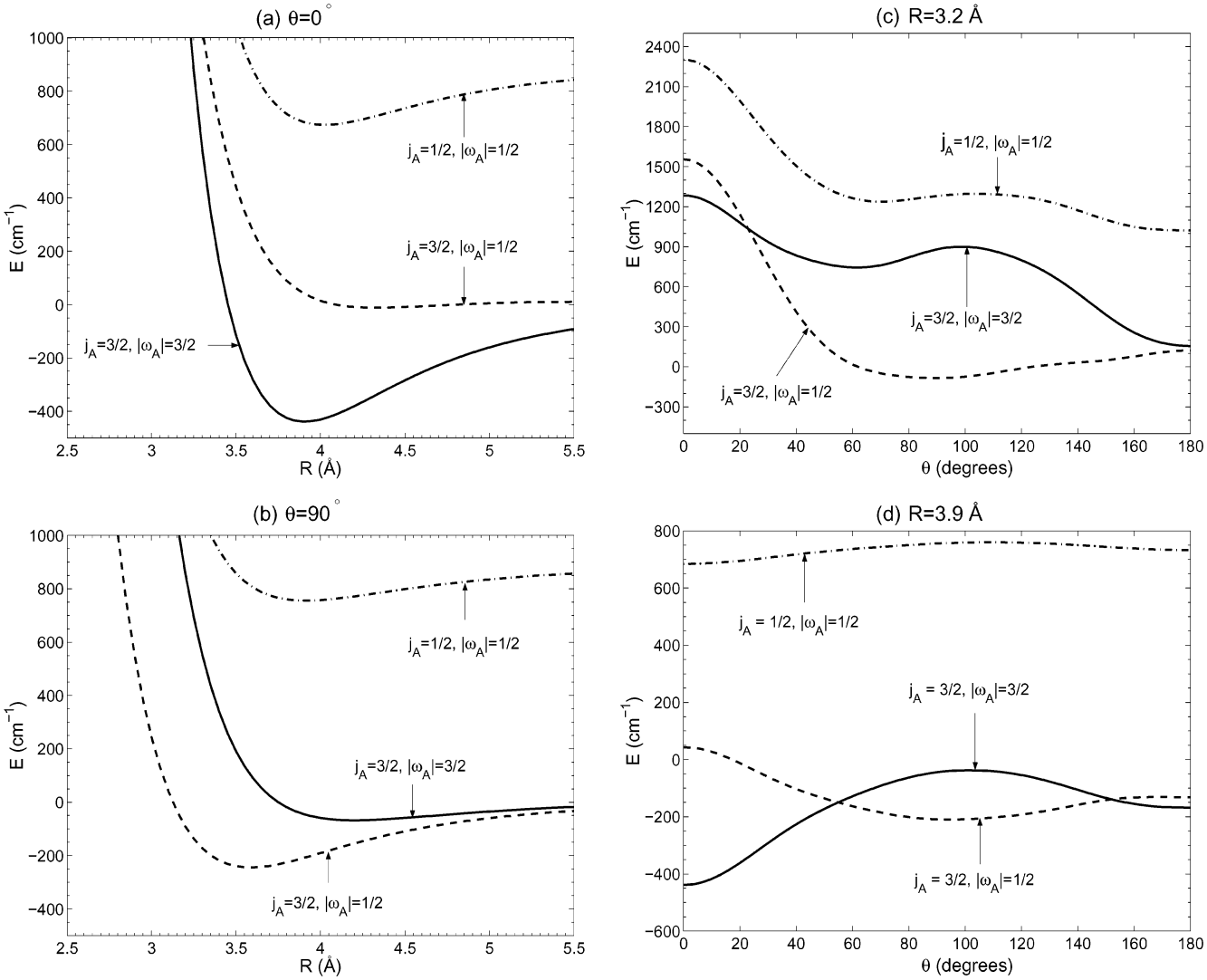

Figure 2. Cuts through the diabatic potential energy surfaces including spin−orbit coupling. Cuts a and b are for $\theta = 0°$ and 90°, respectively; cuts c and d are for $R = 3.2$ and 3.9 Å, respectively.

HCl that one considers also diabatic and adiabatic potential energy surfaces with the large spin−orbit coupling term included. Diabatic states $|j_A\omega_A\rangle$ including spin−orbit coupling are defined, which correlate to the atomic states $|j_A\omega_A\rangle \equiv |(\lambda S)j_A\omega_A\rangle$ of eq 6. The corresponding diabatic potentials $V^{(j_A)}_{\omega'_A,\omega_A}(R,\theta) \equiv \langle j_A\omega'_A|\hat{V} + \hat{H}_{SO}|j_A\omega_A\rangle$ are the matrix elements of the operator

$$\hat{V} + \hat{H}_{SO} = \sum_{\mu',\mu} |\lambda,\mu'\rangle\, V_{\mu',\mu}(R,\theta)\, \langle\lambda,\mu| + A\hat{\boldsymbol{\lambda}}\cdot\hat{\mathbf{S}} \qquad (10)$$

The spin−orbit term is constant and diagonal in this basis. The diagonal elements of the matrix $V^{(j_A)}_{\omega'_A,\omega_A}$ are plotted in Figure 1a−c. Adiabatic potentials are obtained by diagonalization of this matrix and plotted in Figure 1d−f. Similar pictures of their empirical model potential are shown by Dubernet and Hutson.[22] A few of the most relevant cuts through our potential surfaces are presented in Figure 2.

One-Dimensional (1D) Calculations. Before we discuss the full 2D calculation of the bound states, it is useful to consider the hindered internal rotation or bending motion of the HCl monomer in the complex in a series of calculations with fixed Cl−HCl distance R. We made such calculations for values of R ranging from 2.5 to 5.5 Å in steps of 0.1 Å; the energy levels for $J = {}^1/_2$ and $J = {}^3/_2$ are shown in Figure 3. An analysis of the wave functions of the lowest states of parity e is given in Tables 1 and 2, for $R = 3.2$ and 3.9 Å, respectively. Many of the curves in Figure 3 nearly coincide for $J = {}^1/_2$ and ${}^3/_2$, which indicates that the corresponding bound states for $J = {}^3/_2$ are similar to those for $J = {}^1/_2$, except for an additional quantum of overall rotation. In Tables 1 and 2 one can see that $|\Omega|$ is a good approximate quantum number, also for $J = {}^3/_2$, and the nearly coinciding curves correspond to states with $|\Omega| \approx {}^1/_2$. The expansion coefficients of these states are indeed very similar; compare, for example, in Table 1 the lowest state for $J = {}^1/_2$ with the lowest state for $J = {}^3/_2$ and the second state for $J = {}^1/_2$ with the third state for $J = {}^3/_2$. In Table 2 the first and second states for $J = {}^1/_2$ are very similar to the second and fourth states for $J = {}^3/_2$, respectively. The curves in Figure 3 that occur for $J = {}^3/_2$, but not for $J = {}^1/_2$, refer to states with $|\Omega| \approx {}^3/_2$.

An interesting feature observed in Figure 3 is that the lowest energy curve for $J = {}^3/_2$ and $|\Omega| = {}^3/_2$ exhibits two minima, for $R = 3.2$ and 3.9 Å. For $R = 3.2$ Å the lowest level with $J = {}^1/_2$ and $|\Omega| = {}^1/_2$ is the ground state, whereas for $R = 3.9$ Å the ground state has $J = {}^3/_2$ and $|\Omega| = {}^3/_2$. From the potential surface cuts presented in Figure 2a for $\theta = 0°$ and in Figure 2b for 90° one can see that the ground state at 3.2 Å corresponds to a minimum in the lowest diabatic potential with $j_A = {}^3/_2$ and

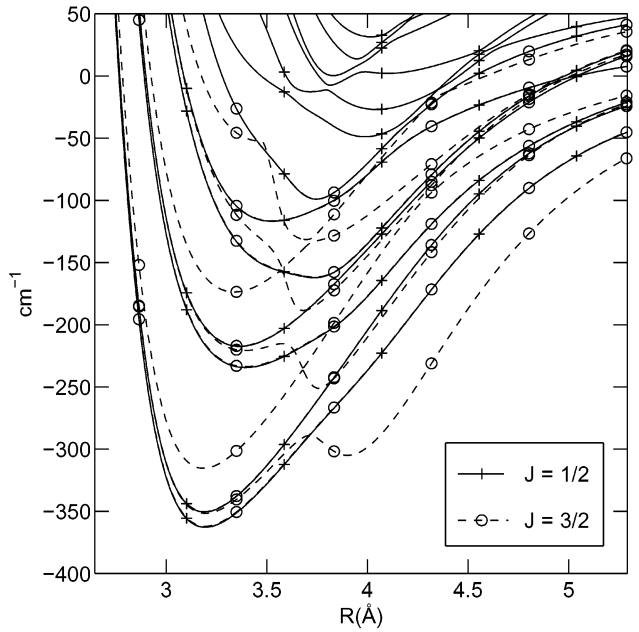

Figure 3. Bound state energies calculated with R fixed at different values. Solid lines with crosses correspond to $J = {}^1/_2$ and dashed lines with circles to $J = {}^3/_2$.

$|\omega_A| = {}^1/_2$ at the T-shaped structure (cf. Figure 1b). It is this diabat that causes the secondary minimum at $\theta = 90°$ in the lowest adiabatic potential energy surface shown in Figure 1d. In Table 1 one observes that the ground state at $R = 3.2$ Å indeed has mostly $j_A = {}^3/_2$ and $|\omega_A| = {}^1/_2$ character. The ground state at $R = 3.9$ Å corresponds to the minimum in the lowest diabat with $j_A = {}^3/_2$ and $|\omega_A| = {}^3/_2$ at the linear structure (see Figure 1a). This diabat is responsible for the minimum at $\theta = 0°$ in the lowest adiabatic potential energy surface shown in Figure 1d. In Table 2 one observes that the ground state at $R = 3.9$ Å indeed has mostly $j_A = {}^3/_2$ and $|\omega_A| = {}^3/_2$ character.

A striking difference between our results and the results of Dubernet and Hutson[22] is that the ground state with the T-shaped structure and $R \approx 3.2$ Å was not found in their calculation. Their lowest adiabatic surface including spin−orbit coupling does not display a minimum for the T-shaped geometry. In their lowest spin-free adiabat they do find a local minimum at the T-shaped structure, but its relative depth in comparison to the global minimum at the linear structure is smaller than in our case (cf. ref 24). Hence, their ground-state resembles the state of linear geometry that we observe around $R = 3.9$ Å. Zdanska et al.[23] did obtain a secondary minimum for the T-shaped structure in their lowest adiabat including spin−orbit coupling, but apparently this minimum is not sufficiently deep to support the T-shaped ground state that we find.

Inspection of the curves in Figure 3 shows an avoided crossing around $R = 3.6$ Å in the lower curves for $J = {}^3/_2$, $|\Omega| = {}^3/_2$. The analysis of the bound states in Tables 1 and 2 shows that this avoided crossing is accompanied by a switch of $|\omega_A| = {}^3/_2$ character at $R = 3.9$ Å, which favors the linear Cl−HCl structure, to $|\omega_A| = {}^1/_2$ character at $R = 3.2$ Å, which favors the T-shaped structure. The approximate quantum number j_A is mostly ${}^3/_2$ for all of the low-lying states, because of the large gap between the $^2P_{3/2}$ and $^2P_{1/2}$ spin−orbit levels in the Cl atom. Still, substantial admixture of the $j_A = {}^1/_2$ component is observed at $R = 3.2$ Å. It is somewhat surprising that $|\omega_A|$ is a nearly good quantum number at $R = 3.2$ Å, but not at $R = 3.9$ Å. This can be understood by looking at the potential surface cuts for $R = 3.2$ Å in Figure 2c, where the $j_A = {}^1/_2$ and $j_A = {}^3/_2$ curves come close for θ around 90° but the $|\omega_A| = {}^1/_2$ and $|\omega_A| = {}^3/_2$ curves with $j_A = {}^3/_2$ stay far apart for $\theta \approx 90°$. In Figure 2d one can see that at $R = 3.9$ Å the $j_A = {}^1/_2$ curve stays far above the $j_A = {}^3/_2$ curves, and the latter stay close together for $|\omega_A| = {}^1/_2$ and $|\omega_A| = {}^3/_2$ over the whole θ range. The diatom rotational quantum number j_B is definitely not a good quantum number; hence, the rotation of HCl is considerably hindered. Surprisingly, one can clearly distinguish states with even j_B and states with odd j_B at $R = 3.2$ Å. Also, $|\omega_B|$ is a nearly good quantum number at $R = 3.2$ Å but not at $R = 3.9$ Å. The exception is the ground state at $R = 3.9$ Å, which we discussed before. It has a linear geometry and $\omega_B \approx 0$. This state can be

TABLE 1: Energies and Wave Functions from 1D Calculations with R Fixed at 3.2 Å[a]

	$J = {}^1/_2$				$J = {}^3/_2$			
E (cm^{-1})	−362.8373	−350.5348	−217.4902	−203.1811	−362.7005	−351.7134	−350.2129	−315.3444
ΔE (cm^{-1})	0.2813	−0.0068	0.2870	−0.0063	0.5625	0.0003	−0.0139	0.0000
$j_A = {}^1/_2$	0.146	0.146	0.135	0.137	0.146	0.145	0.146	0.147
$j_A = {}^3/_2$	0.855	0.854	0.865	0.864	0.855	0.855	0.854	0.853
$\lvert\omega_A\rvert = {}^1/_2$	0.949	0.952	0.959	0.961	0.949	0.948	0.952	0.955
$\lvert\omega_A\rvert = {}^3/_2$	0.051	0.048	0.041	0.039	0.051	0.052	0.048	0.045
$\lvert\Omega\rvert = {}^1/_2$	1.000	1.000	1.000	1.000	1.000	0.027	0.973	0.000
$\lvert\Omega\rvert = {}^3/_2$	0.000	0.000	0.000	0.000	0.000	0.973	0.027	1.000
$j_B = 0$	0.569	0.007	0.051	0.005	0.569	0.018	0.007	0.000
$j_B = 1$	0.046	0.744	0.381	0.058	0.046	0.744	0.744	0.009
$j_B = 2$	0.299	0.055	0.024	0.598	0.299	0.048	0.055	0.825
$j_B = 3$	0.036	0.155	0.424	0.023	0.036	0.152	0.155	0.059
$j_B = 4$	0.037	0.025	0.021	0.264	0.037	0.026	0.025	0.086
$j_B = 5$	0.011	0.010	0.082	0.019	0.011	0.009	0.010	0.016
even j_B	0.906	0.091	0.109	0.894	0.906	0.095	0.091	0.914
odd j_B	0.094	0.909	0.891	0.106	0.094	0.905	0.909	0.086
$\lvert\omega_B\rvert = 0$	0.939	0.018	0.951	0.014	0.939	0.044	0.019	0.000
$\lvert\omega_B\rvert = 1$	0.061	0.941	0.049	0.952	0.061	0.938	0.941	0.018
$\lvert\omega_B\rvert = 2$	0.000	0.041	0.000	0.034	0.000	0.018	0.040	0.943
$\lvert\omega_B\rvert = 3$	0.000	0.000	0.000	0.000	0.000	0.000	0.000	0.039

[a] The energies E refer to the levels of parity e; $\Delta E = E_f - E_e$ is the parity splitting. The contributions of the basis functions with different quantum numbers are sums of squared coefficients.

TABLE 2: Energies and Wave Functions from 1D Calculations with *R* Fixed at 3.9 Å[a]

	$J = {}^1/_2$			$J = {}^3/_2$				
E (cm^{-1})	−255.5538	−227.7538	−193.6043	−305.0698	−255.4367	−231.2392	−227.5604	−182.8490
ΔE (cm^{-1})	0.1383	−0.0013	0.1492	0.0000	0.2766	0.0002	−0.0028	0.0000
$j_A = {}^1/_2$	0.013	0.018	0.010	0.001	0.013	0.015	0.018	0.019
$j_A = {}^3/_2$	0.987	0.983	0.990	0.999	0.987	0.985	0.983	0.981
$\|\omega_A\| = {}^1/_2$	0.599	0.774	0.693	0.069	0.600	0.657	0.774	0.847
$\|\omega_A\| = {}^3/_2$	0.400	0.226	0.308	0.931	0.399	0.343	0.226	0.154
$\|\Omega\| = {}^1/_2$	1.000	1.000	1.000	0.000	1.000	0.002	0.998	0.000
$\|\Omega\| = {}^3/_2$	0.000	0.000	0.000	1.000	0.000	0.998	0.002	1.000
$j_B = 0$	0.445	0.006	0.281	0.220	0.445	0.052	0.006	0.002
$j_B = 1$	0.272	0.679	0.294	0.410	0.271	0.573	0.679	0.008
$j_B = 2$	0.224	0.192	0.173	0.245	0.224	0.169	0.192	0.790
$j_B = 3$	0.055	0.107	0.198	0.085	0.055	0.156	0.107	0.134
$j_B = 4$	0.003	0.015	0.046	0.027	0.003	0.045	0.015	0.059
$j_B = 5$	0.001	0.001	0.006	0.009	0.001	0.005	0.001	0.005
even j_B	0.672	0.213	0.501	0.495	0.673	0.266	0.214	0.852
odd j_B	0.328	0.787	0.499	0.505	0.327	0.734	0.786	0.148
$\|\omega_B\| = 0$	0.597	0.012	0.689	0.930	0.598	0.338	0.013	0.003
$\|\omega_B\| = 1$	0.403	0.767	0.309	0.069	0.402	0.655	0.767	0.013
$\|\omega_B\| = 2$	0.000	0.221	0.001	0.001	0.000	0.007	0.221	0.836
$\|\omega_B\| = 3$	0.000	0.000	0.000	0.000	0.000	0.000	0.000	0.148

[a] The energies E refer to the levels of parity e; $\Delta E = E_f - E_e$ is the parity splitting. The contributions of the basis functions with different quantum numbers are sums of squared coefficients.

considered as a Renner−Teller system, with $|\omega_B|$ being the bending angular momentum that for linear triatomic molecules is commonly denoted l.

Further understanding of these results can be obtained from a view of the angular density distributions plotted in Figures 4 and 5. These distributions are obtained by integrating the absolute square of the rovibronic wave functions over all coordinates except the angle θ. They contain contributions of the different electronic spin−orbit components (j_A,$|\omega_A|$), which are marked separately. It is clear that the Cl atom and the HCl diatom already have a strong interaction at $R = 3.9$ Å, but this affects mostly the diatom by more or less fixing its orientation (j_B is not a good quantum number anymore). The splitting between the $j_A = {}^1/_2$ and $j_A = {}^3/_2$ spin−orbit states of the Cl(^2P) atom is almost completely preserved. For $R = 3.2$ Å there is also a strong change in the spin−orbit levels of the Cl atom and j_A is no longer a good quantum number. Instead, the projections $|\omega_A|$ and $|\omega_B|$ on the intermolecular axis $\boldsymbol{R}$ become good quantum numbers, which shows the more rigid character of the complex.

Figure 4 demonstrates again that the complex forms in the T-shaped geometry at $R = 3.2$ Å. In the ground state, with $\omega_B \approx 0$ (upper left panel), the diatom orientation is more or less fixed around $\theta = 90°$ by a mixture of basis functions with mainly $j_B = 0$ and $j_B = 2$ (see Table 1). In the first excited state, with $|\omega_B| \approx 1$ (upper right panel), the diatom orientation is equally well localized. We mentioned already that the system at $R = 3.2$ Å has a strong preference for even or odd values of j_B. This is reminiscent of the para/ortho distinction in H_2 complexes, but quite unexpected as HCl is a strongly heteronuclear diatom. Even values of j_B occur in the ground state and odd values in the first excited state. Figure 4 also shows that the second and third excited states are bending excited states. For $R = 3.9$ Å (Figure 5), the diatom orientation is clearly more delocalized. This figure contains also the lowest two states with $J = {}^3/_2$ and $|\Omega| = {}^3/_2$. The first one has a linear structure, and the second is delocalized over the linear and T-shaped geometries.

Full Calculation. We performed full two-dimensional (2D) calculations for the intermolecular degrees of freedom by introducing a radial basis of 15 functions $\chi_n(R)$, with $n_{max} = 14$, as defined in ref 30. The nonlinear parameters $R_e = 3.60$ Å, $D_e = 430$ cm^{-1}, and $\omega_e = 34.5$ cm^{-1} in this basis were optimized by energy minimizations with smaller values of n_{max}. The rovibronic levels and parity splittings for $J = {}^1/_2$, ${}^3/_2$, ${}^5/_2$, and ${}^7/_2$ are given in Tables 3 and 4. Also, the main character of the corresponding wave functions is indicated in these tables. As in the calculations with R fixed, $|\Omega|$ is a nearly good quantum number and we can sort the energy levels with respect to $|\Omega|$.

In agreement with the 1D calculations with R fixed at $R = 3.2$ Å we find that the ground state corresponds to the second diabat with $j_A = {}^3/_2$ and $|\omega_A| = {}^1/_2$. The density plots for $J = {}^1/_2$, $|\Omega| = {}^1/_2$ in Figure 6 show that it has a T-shaped geometry. The binding energy D_0 of the complex is 337.8 cm^{-1} for $J = {}^1/_2$, $|\Omega| = {}^1/_2$, and spectroscopic parity e. Note that the lowest adiabatic potential including the spin−orbit coupling displays a local minimum with $D_e = 377$ cm^{-1} at the T-shaped geometry with $R_e = 3.2$ Å, and the zero-point level in the calculations with R fixed at 3.2 Å lies at −362.8 cm^{-1}. The global minimum in this potential with well depth $D_e = 439$ cm^{-1} occurs for the linear geometry at $R_e = 3.9$ Å. The first state with a linear Cl−HCl geometry (see Figure 6, lower two panels) is found for $J = {}^3/_2$, $|\Omega| = {}^3/_2$, and lies at −276.1 cm^{-1}. This is in good agreement with the ground state energy of −273.7 cm^{-1} that Dubernet and Hutson[22] calculated with their empirical model potential. Note that this potential does not support the T-shaped ground state structure, however, which we find much lower in energy. Also, the ab initio potential of Zdanska et al.[23] does not support the T-shaped ground state structure and, moreover, the well depth and binding energy of the complex are considerably smaller in this potential.

We observe in Figure 6 that the angular distributions are in good agreement with the results of the 1D calculations represented in Figures 4 and 5. The states with $J = {}^1/_2$ and $|\Omega| = {}^1/_2$ in Figure 6 correspond to the T-shaped states computed at $R = 3.2$ Å and the states with $J = {}^3/_2$ and $|\Omega| = {}^3/_2$ in Figure 6 to the states of linear geometry found for $R = 3.9$ Å. The states with energies $E = -293.65$ and −279.43 cm^{-1} in Figure

$$J = \tfrac{1}{2}, |\Omega| = \tfrac{1}{2}$$

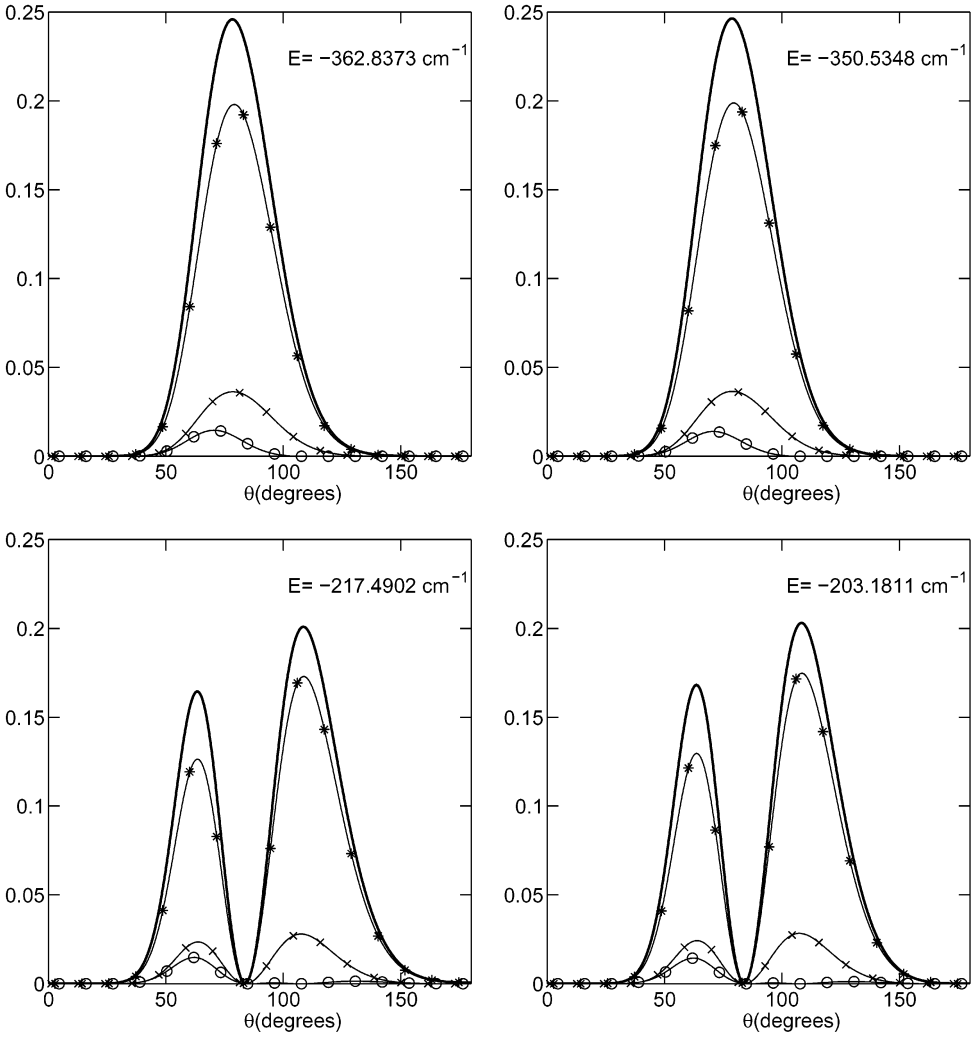

Figure 4. Wave functions squared from 1D calculations at $R = 3.2$ Å for $J = {}^1/_2$, integrated over all coordinates except θ. The contributions of the electronic spin−orbit states (j_A, $|\omega_A|$) are indicated by ○ for ($^3/_2$, $^3/_2$), ∗ for ($^3/_2$, $^1/_2$), and × for ($^1/_2$, $^1/_2$). The energy levels are listed in Table 1.

6 are clearly stretch fundamentals, which have no counterpart in the 1D calculations with R fixed. The states with energies $E = -215.32$ and -197.01 cm^{-1} in Figure 6 are bending fundamentals in nice correspondence with the third and fourth states in Figure 4.

It is clear from Figure 6 that the Cl−HCl complex has two series of states with a T-shaped geometry and $|\Omega| = {}^1/_2$ with very similar internal motion, one with $\omega_B \approx 0$ that includes the ground state at -337.80 cm^{-1} and one with $|\omega_B| \approx 1$ that starts at the slightly higher energy of -325.07 cm^{-1}. In Table 3 one observes two similar series of levels for $|\Omega| = {}^3/_2$, one with $|\omega_B| \approx 1$ starting at -326.93 cm^{-1} and one with $|\omega_B| \approx 2$ starting at -289.53 cm^{-1}. Comparison of the energy levels from the 2D calculation in Table 3 to the levels from the 1D calculation in Table 1 shows that for each of these series of states the stretch zero-point energy of the complex is ~ 25 cm^{-1}. In the harmonic approximation this corresponds to a stretch frequency of ~ 50 cm^{-1}. In the full 2D calculation we could identify stretch progressions with quantum numbers up to $v_s = 4$. Fits of these progressions to the usual formula with anharmonic corrections

$$E(v_s) = D_e + \omega_e\left(v_s + \frac{1}{2}\right) - \omega_e x_e\left(v_s + \frac{1}{2}\right)^2 + \omega_e y_e\left(v_s + \frac{1}{2}\right)^3 \quad (11)$$

yield the spectroscopic parameters listed in Table 5. Two sets of such parameters are given for the T-shaped states with $|\Omega| = {}^1/_2$, one for the states with $\omega_B \approx 0$ and one for the states with $|\omega_B| \approx 1$. The third set of parameters refers to the states with $|\Omega| = {}^3/_2$ and $|\omega_B| \approx 2$. All values of D_e from these fits agree well with the corresponding energies of the 1D calculations at $R = 3.2$ Å. From a comparison of Tables 3 and 2 we extracted a stretch zero-point energy of 29 cm^{-1} for the states of linear geometry with $|\Omega| = {}^3/_2$ and we could identify a stretch progression with the first and second excited states lying at 52.6 and 94.2 cm^{-1}, respectively, above the linear ground state at -276.14 cm^{-1}. A fit of this progression to eq 11 yields a set of parameters for the states of linear geometry with $\omega_B \approx 0$. Again, the value of D_e from the fit agrees well with the lowest energy of the 1D calculation at $R = 3.9$ Å, as it should. The corresponding 2D and 1D bending fundamentals of the T-shaped structure in Tables 3 and 1 do not show a simple stretch zero-point energy shift, nor do the levels in Table 3 show a clear stretch progression on top of the bending excited levels.

The parity splittings of the levels with $J = {}^1/_2$, $^3/_2$, $^5/_2$, and $^7/_2$ are presented in Table 4. They agree very well with the results of the fixed-R calculation at 3.2 Å in Table 1. The largest splittings occur for $|\Omega| = {}^1/_2$, and they are nicely proportional to $J + {}^1/_2$. This simple linear dependence on $J + {}^1/_2$ is well-

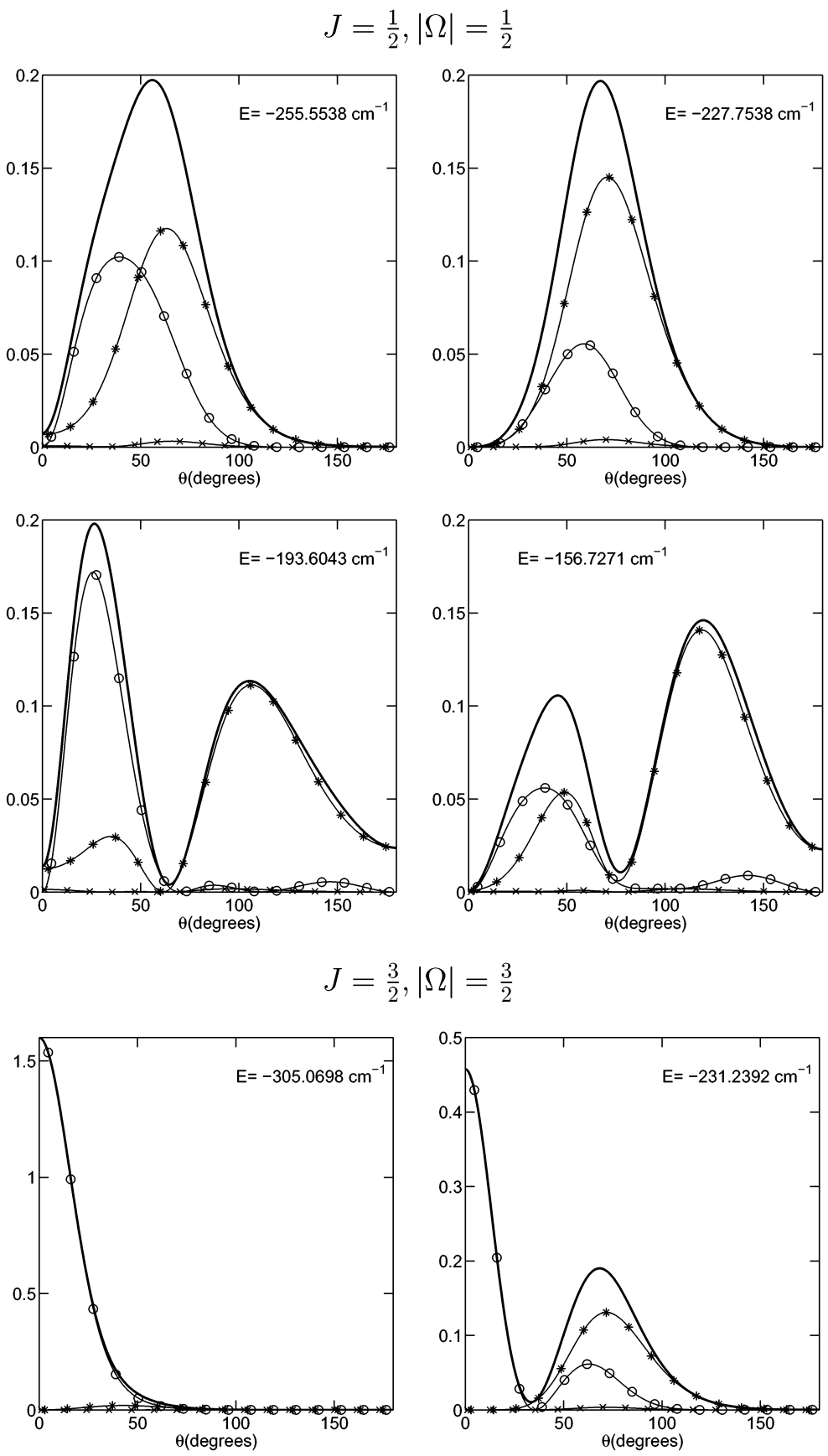

Figure 5. Wave functions squared from 1D calculations at $R = 3.9$ Å, integrated over all coordinates except θ, for $J = {}^1/_2$ (upper four panels) and for $J = {}^3/_2$ (lower two panels). The contributions of the spin−orbit states (j_A, $|\omega_A|$) are indicated by ○ for ($^3/_2$, $^3/_2$), ∗ for ($^3/_2$, $^1/_2$), and × for ($^1/_2$, $^1/_2$). The energy levels are listed in Table 2.

known for λ doubling in linear molecules,[31] and it was also found in Cl(^2P)−HCl by Dubernet and Hutson.[22] For the lowest levels with $\omega_B = 0$ the proportionality constant is on the order of the end-over-end rotational constant (see below). It is

TABLE 3: Lowest Bound States of *e* Parity for $J = {}^1/_2$ up to ${}^7/_2$[a]

$\|\omega_A\|$	$\|\omega_B\|$	v_b	v_s	$J = {}^1/_2$	$J = {}^3/_2$	$J = {}^5/_2$	$J = {}^7/_2$
				$\|\Omega\| = {}^1/_2$			
${}^1/_2$	0	0	0	−337.7954	−337.6639	−337.3530	−336.8627
${}^1/_2$	1	0	0	−325.0662	−324.7655	−324.2682	−323.5761
${}^1/_2$	0	0	1	−293.6461	−293.5216	−293.2286	−292.7672
${}^1/_2$	1	0	1	−279.4261	−279.1678	−278.7404	−278.1451
${}^1/_2$	0	0	2	−254.3481	−254.2233	−253.9404	−253.4994
${}^1/_2$	1	0	2	−237.2569	−237.0075	−236.5930	−236.0137
${}^1/_2$	0	0	3	−220.0136	−219.8837	−219.6032	−219.1720
${}^1/_2$	0	1	0	−215.3239	−215.2127	−214.9421	−214.5123
${}^1/_2$	1	0	3	−198.2722	−197.9996	−197.5585	−196.9534
${}^1/_2$	1	1	0	−197.0106	−196.7601	−196.3435	−195.7608
${}^1/_2$	0	0	4	−187.2257	−187.0933	−186.8135	−186.3863
${}^1/_2$	0	1	1	−182.5825	−182.4678	−182.2048	−181.7934
${}^1/_2$	1	0	4	−161.6095	−161.3869	−161.0068	−160.4702
				$\|\Omega\| = {}^3/_2$			
${}^1/_2$	1	0	0		−326.9326	−326.5281	−325.9594
${}^1/_2$	2	0	0		−289.5309	−289.0560	−288.3921
${}^1/_2$	1	0	1		−286.1012	−285.7228	−285.1937
${}^3/_2$	0	0	0		−276.1414	−275.7858	−275.2856
${}^1/_2$	1	0	2		−243.4595	−243.0580	−242.4980
${}^1/_2$	2	0	1		−241.6363	−241.2266	−240.6514
${}^3/_2$	0	0	1		−223.5215	−223.2030	−222.7569
${}^1/_2$	1	1	1		−202.7512	−202.3781	−201.8561
${}^1/_2$	1	0	3		−200.4761	−200.1142	−199.6072
${}^1/_2$	2	0	2		−198.1769	−197.7996	−197.2593
${}^3/_2$	0	0	2		−181.9647	−181.6557	−181.2231
${}^1/_2$	1	0	4		−165.4738	−165.1164	−164.6162
				$\|\Omega\| = {}^5/_2$			
${}^1/_2$	2	0	0			−292.9108	−292.3186
${}^1/_2$	2	0	1			−250.0382	−249.4693
${}^1/_2$	3	0	0			−231.1916	−230.5332
${}^1/_2$	2	0	2			−214.2311	−213.6980
${}^1/_2$	2	0	3			−184.7843	−184.2657
${}^1/_2$	3	0	1			−182.8027	−182.1994
${}^1/_2$	2	1	0			−161.2700	−160.7185
				$\|\Omega\| = {}^7/_2$			
${}^1/_2$	3	0	0				−236.0136
${}^1/_2$	3	0	1				−192.5597

[a] Energies in cm^{-1} relative to the energy of $Cl(^2P_{3/2})$ and HCl; v_b and v_s are bending and stretch quantum numbers.

remarkable, however, that the $\omega_B = 0$ states for which we find this type of parity splitting in $Cl(^2P)$−HCl are not linear but have a T-shaped geometry. Another characteristic feature is that the parity splitting is much smaller for the levels with $|\omega_B| = 1$. Also, these smaller splittings are proportional to $J + {}^1/_2$, except for the second stretch overtone where some $|\omega_A| = {}^3/_2$ character mixes into the mainly $|\omega_A| = {}^1/_2$ state.

All of these parity splitting characteristics can be understood by considering the Hamiltonian in eq 1 and the parity-adapted basis in eq 9. From the latter it follows that the energy difference between functions with *e* and *f* parities is caused by a coupling between the basis components with $(\omega_A,\omega_B,\Omega)$ and $(-\omega_A,-\omega_B,-\Omega)$. The term in the Hamiltonian that is responsible for this coupling is the Coriolis coupling operator $-2(\hat{\boldsymbol{j}}_A + \hat{\boldsymbol{j}}_B)\cdot\hat{\boldsymbol{J}}/(2\mu_{AB}R^2)$ and, in particular, the step-up and step-down terms with $\hat{j}_A^+\hat{J}^+$ and $\hat{j}_A^-\hat{J}^-$ in this operator. The operator $[\hat{j}_A^z + \hat{j}_B^z]\hat{J}^z$ gives simply $(\omega_A + \omega_B)\Omega = \Omega^2$ for both components of the parity-adapted basis. The step-up and step-down operators $\hat{j}_B^{\pm}\hat{J}^{\pm}$ cannot couple basis functions with ω_B and $-\omega_B$ because this quantum number has integer values and the step-up and step-down operators shift ω_B only by ±1. Hence, only the terms $\hat{j}_A^{\pm}\ \hat{J}^{\pm}/(2\mu_{AB}R^2)$ couple basis functions with $(\omega_A,\omega_B,\Omega) = ({}^1/_2,\ 0,\ {}^1/_2)$ and $(-{}^1/_2,\ 0,\ -{}^1/_2)$. The coupling matrix elements are

TABLE 4: Parity Splittings $\Delta E = E_f - E_e$ in cm^{-1}

$\|\omega_A\|$	$\|\omega_B\|$	v_b	v_s	$J = {}^1/_2$	$J = {}^3/_2$	$J = {}^5/_2$	$J = {}^7/_2$
				$\|\Omega\| = {}^1/_2$			
${}^1/_2$	0	0	0	0.2754	0.5508	0.8261	1.1012
${}^1/_2$	1	0	0	−0.0071	−0.0144	−0.0222	−0.0306
${}^1/_2$	0	0	1	0.2564	0.5127	0.7689	1.0248
${}^1/_2$	1	0	1	−0.0065	−0.0129	−0.0192	−0.0252
${}^1/_2$	0	0	2	0.2245	0.4489	0.6730	0.8967
${}^1/_2$	1	0	2	−0.0031	−0.0062	−0.0095	−0.0129
${}^1/_2$	0	0	3	0.1919	0.3836	0.5749	0.7657
${}^1/_2$	0	1	0	0.2557	0.5115	0.7672	1.0230
${}^1/_2$	1	0	3	0.0044	0.0067	0.0076	0.0076
${}^1/_2$	1	1	0	−0.0036	−0.0075	−0.0118	−0.0166
${}^1/_2$	0	0	4	0.1773	0.3544	0.5312	0.7075
${}^1/_2$	0	1	1	0.2158	0.4280	0.6564	0.8709
${}^1/_2$	1	0	4	0.0281	0.0553	0.0809	0.1046
				$\|\Omega\| = {}^3/_2$			
${}^1/_2$	1	0	0		0.0003	0.0010	0.0024
${}^1/_2$	2	0	0		0.0000	0.0000	0.0000
${}^1/_2$	1	0	1		0.0001	0.0004	0.0009
${}^3/_2$	0	0	0		−0.0001	−0.0005	−0.0012
${}^1/_2$	1	0	2		0.0001	0.0003	0.0008
${}^1/_2$	2	0	1		0.0001	0.0002	0.0005
${}^3/_2$	0	0	1		0.0000	0.0000	0.0000
${}^1/_2$	1	1	1		0.0002	0.0006	0.0015
${}^1/_2$	1	0	3		0.0004	0.0016	0.0039
${}^1/_2$	2	0	2		0.0018	0.0044	0.0073
${}^3/_2$	0	0	2		0.0035	−0.0091	−0.0080
${}^1/_2$	1	0	4		0.0004	0.0017	0.0041

TABLE 5: Spectroscopic Parameters in cm^{-1} from Fits of the Stretch Progressions

$\|\omega_B\|$	$\|\Omega\|$	D_e	ω_e	$\omega_e x_e$	$\omega_e y_e$
0	${}^1/_2$	−362.6657	51.5924	4.0430	0.2754
1	${}^1/_2$	−349.4424	49.8261	2.2280	0.0957
2	${}^3/_2$	−315.1439	52.5612	2.6273	0.1378
0	${}^3/_2$	−306.6001	63.6830	5.5315	

$$\sqrt{(j_A(j_A+1) - \omega_A(\omega_A \pm 1))(J(J+1) - \Omega(\Omega \pm 1))} \times \langle[2\mu_{AB}R^2]^{-1}\rangle = \left(j_A + \frac{1}{2}\right)\left(J + \frac{1}{2}\right)\langle[2\mu_{AB}R^2]^{-1}\rangle \quad (12)$$

and they cause a first-order splitting between the functions of *e* and *f* parities, which would otherwise be degenerate. Equation 12 shows that this splitting should indeed be proportional to $J + {}^1/_2$, with a proportionality constant that is $2(j_A + {}^1/_2)$ times the expectation value of $[2\mu_{AB}R^2]^{-1}$ over the radial part of the wave function. The quantum number j_A is mostly ${}^3/_2$ in the lower levels, and the expectation value $\langle[2\mu_{AB}R^2]^{-1}\rangle$ is the end-over-end rotational constant *B* of the complex. In reality, the parity splitting for the states with $\omega_B \approx 0$ is somewhat smaller than 4*B*. Functions with $\omega_B \neq 0$ are not coupled and would not show any parity splitting if ω_B were an exact quantum number. It is not exact, however, so even the wave functions with $|\omega_B| \approx 1$ have a small component with $\omega_B = 0$ and show a small parity splitting. For $|\Omega| = {}^3/_2$ the splittings are even smaller, and they are proportional to $(J - {}^1/_2)(J + {}^1/_2)(J + {}^3/_2)$ as pointed out by Dubernet and Hutson.[22] They are due to a higher order effect of the Coriolis coupling operator $\hat{j}_A^{\pm}\ \hat{J}^{\pm}/(2\mu_{AB}R^2)$. No splittings are shown for $|\Omega| > {}^3/_2$ because they are hardly visible at the accuracy of our calculations.

From the levels with $J = {}^1/_2$, ${}^3/_2$, ${}^5/_2$, and ${}^7/_2$ we extracted rotational constants of the complex. First, we averaged the energies of the *e* and *f* states to remove the effect of the parity splitting. We note that the *J* dependence of the energy levels originates from the term $[(\hat{\boldsymbol{j}}_A + \hat{\boldsymbol{j}}_B)^2 - 2(\hat{\boldsymbol{j}}_A + \hat{\boldsymbol{j}}_B)\cdot\hat{\boldsymbol{J}} + \hat{J}^2]/(2\mu_{AB}R^2)$ in the Hamiltonian. After removal of the parity splitting, the energy contribution of this term is $[J(J+1) - \Omega^2]\langle[2\mu_{AB}R^2]^{-1}\rangle$.

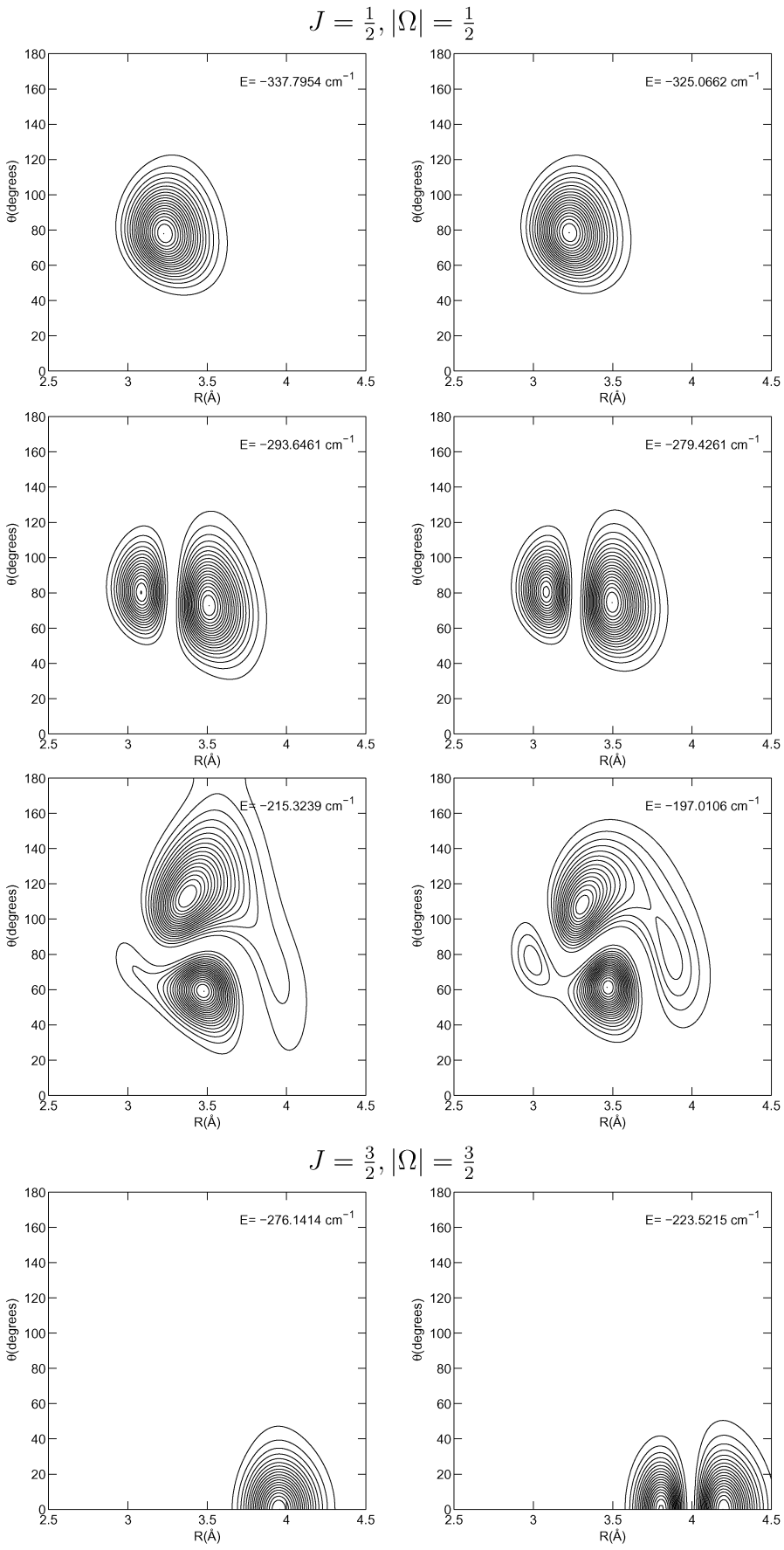

Figure 6. Density distributions from full 2D calculations for $J = {}^1/_2$ and $|\Omega| = {}^1/_2$ (upper six panels) and for $J = {}^3/_2$ and $|\Omega| = {}^3/_2$ (lower two panels). These distributions are the squares of the rovibronic wave functions, integrated over the electronic coordinates and the overall rotation angles of the complex (α, β, ϕ). The corresponding energy levels are listed in Table 3.

TABLE 6: Expectation Values and Spectroscopic Parameters in cm^{-1} from Fits of the Rotational Levels

$\|\omega_A\|$	$\|\omega_B\|$	v_b	v_s	$\langle R\rangle$ (Å)	B_{av}	E_0	B	D
				$\|\Omega\| = {}^1/_2$				
$^1/_2$	0	0	0	3.26	0.09013	−337.70	0.08972	8.70×10^{-7}
$^1/_2$	1	0	0	3.25	0.09045	−325.12	0.09912	3.53×10^{-5}
$^1/_2$	0	0	1	3.38	0.08466	−293.56	0.08423	1.64×10^{-6}
$^1/_2$	1	0	1	3.36	0.08541	−279.47	0.08511	2.04×10^{-5}
$^1/_2$	0	0	2	3.51	0.07946	−254.28	0.07901	1.50×10^{-6}
$^1/_2$	1	0	2	3.47	0.08114	−237.30	0.08263	4.88×10^{-6}
$^1/_2$	0	0	3	3.61	0.07564	−219.96	0.07526	1.79×10^{-6}
$^1/_2$	0	1	0	3.47	0.07973	−215.24	0.07970	1.27×10^{-6}
$^1/_2$	1	0	3	3.53	0.07863	−198.31	0.09134	2.11×10^{-4}
$^1/_2$	1	1	0	3.46	0.08052	−197.05	0.08286	-1.34×10^{-6}
$^1/_2$	0	0	4	3.67	0.07392	−187.17	0.07366	1.60×10^{-6}
$^1/_2$	0	1	1	3.62	0.07446	−182.51	0.07491	2.26×10^{-5}
$^1/_2$	1	0	4	3.61	0.07593	−161.63	0.07881	1.91×10^{-5}
				$\|\Omega\| = {}^3/_2$				
$^1/_2$	1	0	0	3.26	0.08995	−327.05	0.08071	-3.23×10^{-5}
$^1/_2$	2	0	0	3.25	0.09050	−289.67	0.09506	1.06×10^{-5}
$^1/_2$	1	0	1	3.54	0.07765	−286.21	0.07573	4.99×10^{-6}
$^3/_2$	0	0	0	3.75	0.06968	−276.25	0.07090	-2.48×10^{-5}
$^1/_2$	1	0	2	3.49	0.08054	−243.58	0.08050	2.30×10^{-5}
$^1/_2$	2	0	1	3.44	0.08237	−241.76	0.08178	-2.07×10^{-5}
$^3/_2$	0	0	2	3.91	0.06396	−223.62	0.06368	-2.34×10^{-6}
$^1/_2$	1	1	0	3.55	0.07718	−202.86	0.07468	1.67×10^{-6}
$^1/_2$	1	1	1	3.54	0.07789	−200.58	0.07242	-8.87×10^{-6}
$^1/_2$	2	0	2	3.48	0.08088	−198.29	0.07459	-1.40×10^{-4}
$^3/_2$	0	0	3	4.00	0.06187	−182.05	0.05964	-1.12×10^{-4}
$^1/_2$	1	0	4	3.62	0.07532	−165.58	0.07159	-1.99×10^{-6}

The band origins E_0, end-over-end rotational constants B, and centrifugal distortion constants D presented in Table 6 were obtained by a fit of the levels with $J = {}^1/_2$, ${}^3/_2$, ${}^5/_2$, and ${}^7/_2$ for each internal state with the formula

$$E(J,|\Omega|) = E_0 + B(J(J+1) - \Omega^2) - D(J(J+1) - \Omega^2)^2 \quad (13)$$

From the wave function of each state we also calculated the expectation value of R and the rotational constant $B_{av} = \langle[2\mu_{AB}R^2]^{-1}\rangle$. In Table 6 we compare these results. Especially for the levels with $\omega_B = 0$ we find that the B value from the fit of the rotational levels agrees very well with the expectation value B_{av}. The agreement is somewhat less good for the levels with $|\omega_B| = 1$. In the fit with eq 13 it is assumed that the complex is a linear rotor. Hence, we may conclude that the states with $\omega_B = 0$ behave as a linear rotor, whereas the states with $|\omega_B| = 1$ do not. This conclusion is quite remarkable, however, because the complex has clearly a T-shaped geometry, even in the states with $\omega_B = 0$. The same conclusion was reached on the basis of the parity splittings.

In the rotational constants and the values of $\langle R\rangle$ in Table 6 one observes a marked distinction between the T-shaped and linear structures. All of the states with $|\Omega| = {}^1/_2$ have a relatively large rotational constant and $\langle R\rangle$ values between 3.2 and 3.5 Å. They are T-shaped. For $|\Omega| = {}^3/_2$ we find T-shaped states with $|\omega_A| \approx {}^1/_2$ and linear states with $|\omega_A| \approx {}^3/_2$. The latter have a substantially smaller rotational constant B and a value of $\langle R\rangle$ between 3.7 and 4.0 Å. The value of B for the linear geometry agrees fairly well with the value of Dubernet and Hutson.[22]

Conclusion

Without consideration of the spin−orbit coupling the Cl(^2P)−HCl complex has three asymptotically degenerate electronic states. With the use of the accurate ab initio adiabatic and diabatic intermolecular potential energy surfaces that were recently computed for these states,[24] we calculated the bound levels of this complex for $J = {}^1/_2$, ${}^3/_2$, ${}^5/_2$, and ${}^7/_2$ with the inclusion of spin−orbit coupling. After a fit of the diabatic potentials with an appropriate analytic form of the anisotropy, we present diabatic and adiabatic potentials including spin−orbit coupling. These were very useful in understanding the characteristics of the bound levels calculated. We further elucidated these characteristics by a series of 1D calculations on the hindered rotation or bending motion of the HCl monomer with the Cl−HCl distance R fixed at values ranging from 2.5 to 5.5 Å. The ground state of the complex turned out to have a T-shaped geometry with $\langle R\rangle \approx 3.2$ Å, and we identified the associated stretch and bending excited levels. We also found a progression of states with a linear geometry of the complex at substantially higher energy with $\langle R\rangle \approx 3.7-4.0$ Å. Previous, more approximate, calculations with empirical[22] or ab initio[23] potentials led to a ground state of linear geometry; the T-shaped states were not predicted in earlier work. Stretch and bending vibrational frequencies, rotational constants, and parity splittings were obtained from the usual spectroscopic fits of the levels calculated for different values of J; the rotational constants were also computed from expectation values. It is noteworthy that the Cl−HCl complex displays several series of states with a T-shaped geometry and very similar internal motion, with different values of $|\omega_B|$. This quantum number ω_B is the component of rotational angular momentum j_B of the HCl monomer on the Cl−HCl bond axis. The series of levels with $\omega_B \approx 0$ includes the ground state and has the remarkable feature that the states possess a T-shaped structure, but display several of the properties of a linear open-shell molecule, such as a relatively large parity splitting proportional to $J + {}^1/_2$.

Acknowledgment. This research has been financially supported by the Council for Chemical Sciences of The Netherlands Organization for Scientific Research (CW-NWO). J.K. also acknowledges support from the European Research Training Network THEONET II and from the Polish Committee for Scientific Research KBN (Grant 3 T09A 112 18). We thank Dr. P. E. S. Wormer for useful comments on the manuscript.

References and Notes

(1) Schatz, G. C. *J. Chem. Phys.* **1989**, *90*, 3582.
(2) Gadzy, B.; Bowman, J. M. *J. Chem. Phys.* **1989**, *91*, 4615.
(3) Schatz, G. C.; Sokolovski, D.; Connor, J. N. L. *Faraday Discuss. Chem. Soc.* **1991**, *91*, 17.
(4) Yamashita, K.; Morokuma, K. *J. Chem. Phys.* **1990**, *93*, 3716.
(5) Hahn, O.; Gomez, J. M. L.; Taylor, S. H. *J. Chem. Phys.* **1991**, *94*, 2608.
(6) Whiteley, T. W. J.; Dobbyn, A. J.; Connor, J. N. L.; Schatz, G. C. *Phys. Chem. Chem. Phys.* **2000**, *2*, 549.
(7) Dobbyn, A. J.; Connor, J. N. L.; Besley, N. A.; Knowles, P. J.; Schatz, G. C. *Phys. Chem. Chem. Phys.* **1999**, *1*, 957.
(8) González, M.; Hijazo, J.; Novoa, J. J.; Sayós, R. *J. Chem. Phys.* **1998**, *108*, 3168.
(9) Schatz, G. C.; McCabe, P.; Connor, J. N. L. *Faraday Discuss.* **1998**, *110*, 139.
(10) Maierle, C. S.; Schatz, G. C.; Gordon, M. S.; McCabe, P.; Connor, J. N. L. *J. Chem. Soc., Faraday Trans.* **1997**, *93*, 709.
(11) Bondi, D. K.; Connor, J. N. L.; Manz, J.; Römelt, J. *Mol. Phys.* **1983**, *50*, 467.
(12) Connor, J. N. L.; Jakubetz, W. In *Supercomputer Algorithms for Reactivity, Dynamics and Kinetics of Small Molecules*; Laganà, A., Ed.; Kluwer: Dordrecht, The Netherlands, 1989; pp 395−411.
(13) Sun, Q.; Bowman, J. M.; Schatz, G. C.; Sharp, J. R.; Connor, J. N. L. *J. Chem. Phys.* **1990**, *92*, 1677.
(14) Schatz, G. C.; Amaee, B.; Connor, J. N. L. *J. Chem. Phys.* **1990**, *92*, 4893.
(15) Fulmer, J. P.; Aker, P. M. *J. Chem. Phys.* **1992**, *96*, 4252.
(16) Jakubetz, W.; Sokolovski, D.; Connor, J. N. L.; Schatz, G. C. *J. Chem. Phys.* **1992**, *97*, 6451.
(17) Cohen, M. J.; Willets, A.; Handy, N. C. *J. Chem. Phys.* **1993**, *99*, 5885.
(18) Metz, R. B.; Kitsopoulos, T.; Weaver, A.; Neumark, D. M. *J. Chem. Phys.* **1988**, *88*, 1463.
(19) Metz, R. B.; Weaver, A.; Bradforth, S. E.; Kitsopoulos, T. N.; Neumark, D. M. *J. Phys. Chem.* **1990**, *94*, 1377.
(20) Neumark, D. M. *Annu. Rev. Phys. Chem.* **1992**, *43*, 153.
(21) Skouteris, D.; Manolopoulos, D. E.; Bian, W.; Werner, H. J.; Lai, L.-H.; Liu, K. *Science* **1999**, *286*, 1713.
(22) Dubernet, M.-L.; Hutson, J. *J. Phys. Chem.* **1994**, *98*, 5844.
(23) Žďánska, P.; Nachtigallová, D.; Nachtigall, P.; Jungwirth, P. *J. Chem. Phys.* **2001**, *115*, 5974.
(24) Kłos, J.; Chałasiński, G.; Szczęśniak, M. M.; Werner, H.-J. *J. Chem. Phys.* **2001**, *115*, 3085.
(25) Alexander, M. H. *J. Chem. Phys.* **1993**, *99*, 6014.
(26) Dubernet, M.-L.; Hutson, J. *J. Chem. Phys.* **1994**, *101*, 1939.
(27) Zeimen, W. B.; Kłos, J. A.; Groenenboom, G. C.; van der Avoird, A. *J. Chem. Phys.* **2003**, *118*, 7340.
(28) Esposti, A. D.; Werner, H.-J. *J. Chem. Phys.* **1990**, *93*, 3351.
(29) Tang, K. T.; Toennies, J. P. *J. Chem. Phys.* **1984**, *80*, 3726.
(30) Tennyson, J.; Sutcliffe, B. T. *J. Chem. Phys.* **1982**, *77*, 4061.
(31) Lefebvre-Brion, H.; Field, R. W. *Perturbations in the Spectra of Diatomic Molecules*; Academic Press: New York, 1986.